latoxin moiety is oriented such that the guanine in the complementary strand is sterically inaccessible to attack by epoxide **2**; i.e., the presence of AFB1 covalently linked to one guanine in $d(ATCGAT)_2$ precludes a second molecule of AFB1 epoxide from achieving the transition state with the other guanine. Intercalation of the aflatoxin moiety in adduct **3** above the 5′ face of the modified guanine would be consistent with this observation and represents an attractive hypothesis with which to explain the observed stoichiometry of adduct formation. Thus, existing experimental data regarding the geometry of the associative AFB1–$d(ATCGAT)_2$ complex and of covalent adduct **3** are similar and more consistent with intercalation than with groove binding. It therefore seems plausible that the transition state for reaction of epoxide **2** with DNA, although not directly observable, also involves intercalation.

The accessibility of chemically discrete AFB1–oligodeoxynucleotide adducts will now permit detailed conformational analysis by NMR spectroscopy. Further study of adduct **3** will establish its three-dimensional structure with certainty.

**Acknowledgment.** This research has been funded by the National Institutes of Health, Grants ES-03755 and ES-00267. We thank Professor Fu-Ming Chen (Tennessee State University) for providing assistance in obtaining CD spectra and Dr. Steven W. Baertschi for advice on preparation of dimethyldioxirane and epoxide **2**.

# Mössbauer Analysis of the Binuclear Iron Site in Purple Acid Phosphatase from Pig Allantoic Fluid

**J. T. Sage,[1a,b] Y.-M. Xia,[1a] P. G. Debrunner,*[,1a] D. T. Keough,[1c] J. de Jersey,[1c] and Burt Zerner*[,1c]**

*Contribution from the Department of Physics, University of Illinois, Urbana, Illinois 61801, and the Department of Biochemistry, University of Queensland, St. Lucia, Queensland, Australia 4067.* *Received March 29, 1988*

**Abstract:** We present a quantitative analysis of the Mössbauer spectra of the spin-coupled two-iron center in porcine purple acid phosphatase. The active enzyme contains a high-spin Fe(III)–Fe(II) pair with a ground state of effective spin $S = {}^1/_2$ and **g** tensor $g = (1.56, 1.72, 1.93)$, while the oxidized, inactive enzyme contains a high-spin Fe(III)–Fe(III) pair with a diamagnetic ground state. The Mössbauer spectra of reduced enzyme recorded at 4.2 K show complex magnetic hyperfine splittings, which have been parametrized in terms of the spin Hamiltonian $H = \beta \mathbf{S} g \mathbf{B} + \sum_i \mathbf{S} A_i \mathbf{I}_i + \sum_i \mathbf{I}_i P_i \mathbf{I}_i - \sum_i \beta_N g_N \mathbf{I}_i \mathbf{B}$, $S = {}^1/_2$, where $i$ = A and B labels the ferric and ferrous site, respectively. The fitting parameters **g** and $A_i$ can, in turn, be related to the intrinsic tensors $g_i$ and $a_i$ of the ferric and ferrous ions, respectively, assuming the coupling $H = -2J\mathbf{S}_A\mathbf{S}_B + \sum_i \mathbf{S}_i D_i \mathbf{S}_i$ between the intrinsic spins $S_A = {}^5/_2$ and $S_B = 2$. With the estimate $-2J = 20$ cm$^{-1}$ (Lauffer et al. *J. Biol. Chem.* **1983**, *258*, 14212–14218) and reasonable zero-field splittings $D_i$, the model explains the low $g$ values and the unusual anisotropy of the ferric hyperfine tensor $A_A$ in the coupled representation. Explicit expressions for the tensors **g** and $A_i$ are given to first order in $D_i/J$. this intermediate coupling model, $|D_i/J| \lesssim 1$, is likely to apply to semimethemerythrins, methane monooxygenase, and other high-spin Fe(III)–Fe(II) couples with **g** values differing widely from $g = 2$ and to hold the key to a quantitative interpretation of susceptibility, ENDOR, and other magnetic properties. Preliminary data for metal-substituted and differentially enriched phosphatase are also presented. The parameters of the iron in the Fe–Zn enzyme are found to be close to the intrinsic parameters deduced from the analysis of the native Fe(III)–Fe(II) enzyme, a result that not only corroborates our model but also indicates little change in the iron environment on substitution of zinc. This result further suggests that in mixed-metal clusters the intrinsic properties of each iron site can be studied without the complexities arising from the exchange coupling.

There is increasing evidence for a new group of binuclear metalloenzymes, the purple acid phosphatases (PAP),[2-12] and much effort has been devoted to their characterization.[13-25] Isolated from mammals[2,4,5] and plants,[6,12] these glycoproteins have a unique active site comprising two interacting metal

(1) (a) University of Illinois. (b) Current address: Physics Department, Northeastern University, Boston, MA 02115. (c) University of Queensland.
(2) Glomset, J.; Porath, J. *Biochim. Biophys. Acta* **1960**, *39*, 1–8.
(3) Jacobs, M. M.; Nyc, J. F.; Brown, D. M. *J. Biol. Chem.* **1971**, *246*, 1419–1425.
(4) Campbell, H. D.; Zerner, B. *Biochem. Biophys. Res. Commun.* **1973**, *54*, 1498–1503.
(5) Schlosnagle, D. C.; Bazer, F. W.; Tsibris, J. C. M.; Roberts, R. M. *J. Biol. Chem.* **1974**, *249*, 7574–7579.
(6) Uehara, K.; Fujimoto, S.; Taniguchi, T. *J. Biochem.* **1974**, *75*, 627–38.
(7) Davis, J. C.; Lin, S. S.; Averill, B. A. *Biochemistry* **1981**, *20*, 4062–4067.
(8) Antanaitis, B. C.; Aisen, P. *Adv. Inorg. Biochem.* **1983**, *5*, 111–136.
(9) Andersson, G.; Ek-Rylander, B.; Hammarstrom, L. *Arch. Biochem. Biophys.* **1984**, *228*, 431–438.
(10) Hara, A.; Savada, H.; Kato, T.; Nakayama, T.; Yamamoto, H.; Matsumoto, Y. *J. Biochem.* **1984**, *95*, 67–74.
(11) Roberts, R. M.; Bazer, F. W. *Bioessays* **1984**, *1*, 8–11. While the pig allantoic fluid purple acid phosphatase has been called uteroferrin, there is little evidence in support of the implied function.
(12) Beck, J. L.; McConachie, L. A.; Summors, A. S.; Arnold, W. M.; de Jersey, J.; Zerner, B. *Biochim. Biophys. Acta* **1986**, *869*, 61–68.
(13) Campbell, H. D.; Dionysius, D. A.; Keough, D. T.; Wilson, B. W.; de Jersey, J.; Zerner, B. *Biochem. Biophys. Res. Commun.* **1978**, *82*, 615–620.
(14) Gaber, B. P.; Sheridan, J. P.; Bazer, F. W.; Roberts, R. M. *J. Biol. Chem.* **1979**, *254*, 8340–8342.
(15) Keough, D. T.; Dionysius, D. A.; de Jersey, J.; Zerner, B. *Biochem. Biophys. Res. Commun.* **1980**, *94*, 600–605.
(16) Keough, D. T.; Beck, J. L.; de Jersey, J.; Zerner, B. *Biochem. Biophys. Res. Commun.* **1982**, *108*, 1643–1648.
(17) Antanaitis, B. C.; Strekas, T.; Aisen, P. *J. Biol. Chem.* **1982**, *257*, 3766–3770.
(18) Antanaitis, B. C.; Aisen, P. *J. Biol. Chem.* **1982**, *257*, 5330–5332.
(19) Davis, J. C.; Averill, B. A. *Proc. Natl. Acad. Sci. U.S.A.* **1982**, *79*, 4623–4627.
(20) Antanaitis, B. C.; Aisen, P.; Lilienthal, H. R. *J. Biol. Chem.* **1983**, *258*, 3166–3172.
(21) Lauffer, R. B.; Antanaitis, B. C.; Aisen, P.; Que, L., Jr. *J. Biol. Chem.* **1983**, *258*, 14212–14218.
(22) Debrunner, P. G.; Hendrich, M. P.; de Jersey, J.; Keough, D. T.; Sage, J. T.; Zerner, B. *Biochim. Biophys. Acta* **1983**, *745*, 103–106.
(23) Beck, J. L.; Keough, D. T.; de Jersey, J.; Zerner, B. *Biochim. Biophys. Acta* **1984**, *791*, 357–363.
(24) Antanaitis, B. A.; Peisach, J.; Mims, W. B.; Aisen, P. *J. Biol. Chem.* **1985**, *260*, 4572–4574.

0002-7863/89/1511-7239$01.50/0 

ions[7,12,13,15,19,20,25] with unusual magnetic properties.[18,19,22,25-28] Tyrosinate coordination to at least one of the metals gives rise to characteristic optical transitions with bands between 500 and 550 nm.[14,17] The physiological role of these proteins is not known,[11] but they all show high phosphatase activity with a maximum near pH 4.9.[4,8] The two metals of the active site are typically iron, but a Zn–Fe[12,29] and a Mn enzyme[30] with otherwise similar properties have been reported. The best-characterized PAPs are those isolated from beef spleen[4,7,13,18,19,31] and pig allantoic fluid.[5,13,15,20,21,32] Both proteins have molecular masses of 35–40 kDa and contain a binuclear iron center of as yet unknown structure,[13,22,26,28,31,33] which is characterized by a low-temperature EPR signal with $g \sim (1.59, 1.74, 1.93)$.[7,19,20,25]

The porcine enzyme, also called uteroferrin,[11,34] is the subject of this study. Binding of phosphate or similar oxyanions modifies the optical and magnetic properties of the active site.[7,16,20,24,28,35,36] Oxidation by one electron changes the optical spectrum and abolishes both phosphatase activity and the "$g \sim 1.72$" EPR signal.[13,19,25,28,31] Both irons can be exchanged,[22,28] and protein reconstituted with iron and zinc retains phosphatase activity.[15,19,23,37] Earlier Mössbauer experiments have shown the two irons to have high spin, forming a Fe(III)–Fe(II) pair with an effective spin of $S = {}^1/_2$ in the ground state of the active enzyme and a nonequivalent Fe(III)–Fe(III) pair with a ground state spin of $S = 0$ in the oxidized, inactive enzyme.[22,31,38] Susceptibility measurements suggest an exchange interaction of $-2J \sim 20$ cm$^{-1}$ in the Fe(III)–Fe(II) pair and $-2J \geq 80$ cm$^{-1}$ in the Fe(III)–Fe(III) pair,[21,46] where the constant $J$ is defined by the Hamiltonian $H = -2J\mathbf{S}_A\mathbf{S}_B$. NMR spectroscopy implicates histidine ligands of the iron in addition to tyrosine,[21] a finding compatible with ENDOR and electron spin-echo data.[24] Striking similarities between the iron centers of PAPs and the functionally unrelated hemerythrins[39] are apparent in their magnetic properties[40,41] and their Mössbauer parameters.[22,38,41] It is generally assumed that the two binuclear clusters have structural similarities as well, such as a $\mu$-hydroxo or $\mu$-oxo bridge linking the irons.[31,42,43] More recently, similar EPR and Mössbauer spectra have been found in methane monooxygenase as well.[44]

**Scheme I**[a]

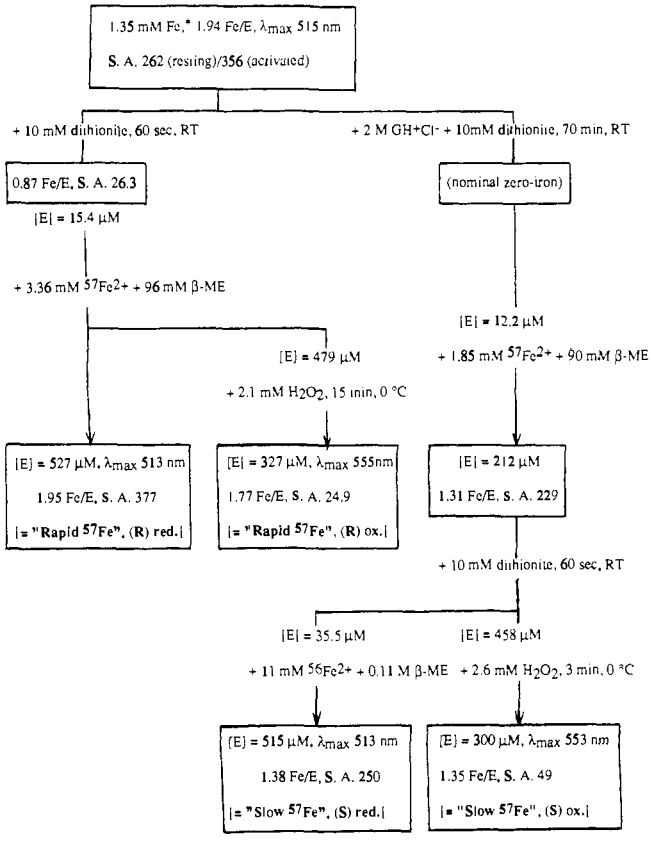


[a] Fe* denotes total iron concentration of enzyme sample.

Here we present new Mössbauer results on the active, reduced and the inactive, oxidized forms of PAP. We have analyzed the complex magnetic hyperfine splittings of the spin $S = {}^1/_2$ Fe(III)–Fe(II) cluster recorded at low temperatures and propose a spin-coupling model that includes the zero-field splitting of the individual sites as well as an isotropic exchange interaction.[38] The model relates the intrinsic magnetic moments and hyperfine tensors to the effective values observed in the spin-coupled ground state and explains the unusual $g$ tensor, the low-temperature susceptibility,[45] and the anisotropy of the magnetic hyperfine coupling in a consistent way. In addition, we present more detailed data on the anomalous thermal broadening of the Mössbauer lines in the Fe(III)–Fe(III) cluster.[22] This type of behavior occurs also in the corresponding phosphate complex of PAP but has otherwise rarely been noticed before.[46a-g]

Next, we briefly summarize EPR and Mössbauer data of Zn- and Hg-substituted samples[23] and show that the parameters observed for the Fe(III) site compare favorably with the intrinsic parameters of the A site, as deduced from our model for the native enzyme. The substitution of Zn or Hg for Fe(II) apparently leaves the coordination of the A site intact.

Finally, we discuss attempts to enrich the two iron sites differentially. Although the differential enrichment in $^{57}$Fe was small,

(25) Antanaitis, B. C.; Aisen, P.; Lilienthal, H. R.; Roberts, R. M.; Bazer, F. W. *J. Biol. Chem.* **1980**, *255*, 11204–11209.
(26) Sinn, E.; O'Connor, C. J.; de Jersey, J.; Zerner, B. *Inorg. Chim. Acta* **1983**, *78*, 13–15.
(27) Antanaitis, B. C.; Aisen, P. *J. Biol. Chem.* **1982**, *257*, 1855–1859.
(28) Pyrz, J. W.; Sage, J. T.; Debrunner, P. G.; Que, L., Jr. *J. Biol. Chem.* **1986**, *261*, 11015–11020.
(29) King, M. M.; Huang, C. Y. *J. Biol. Chem.* **1984**, *259*, 8847–8856.
(30) Sugiura, Y.; Kawabe, H.; Tanaka, H. J. *J. Am. Chem. Soc.* **1980**, *102*, 6582–6584.
(31) Averill, B. A.; Davis, J. C.; Burman, S.; Zirino, T.; Sanders-Loehr, J.; Loehr, T. M.; Sage, J. T.; Debrunner, P. G. *J. Am. Chem. Soc.* **1987**, *109*, 3760–3767.
(32) Bazer, F. W.; Chen, T. T.; Knight, J. W.; Schlosnagle, D. C.; Baldwin, N. J.; Roberts, R. M. *J. Anim. Sci.* **1975**, *41*, 1112–1119.
(33) Antanaitis, B. C.; Aisen, P. *J. Biol. Chem.* **1984**, *259*, 2066–2069.
(34) Buhi, W. C.; Ducsay, C. A.; Bazer, F. W.; Roberts, R. M. *J. Biol. Chem.* **1982**, *257*, 1712–1723.
(35) Antanaitis, B. C.; Aisen, P. *J. Biol. Chem.* **1985**, *260*, 751–756.
(36) Burman, S.; Davis, J. C.; Weber, M. J.; Averill, B. A. *Biochem. Biophys. Res. Commun.* **1986**, *136*, 490–497.
(37) Buhi, W. C.; Gray, W. J.; Mansfield, E. A.; Chun, P. W.; Ducsay, C. A.; Bazer, F. W.; Roberts, R. M. *Biochim. Biophys. Acta* **1982**, *701*, 32–38.
(38) Sage, J. T.; Debrunner, P. G. *Hyperfine Interact.* **1986**, *29*, 1399–1402.
(39) Wilkins, R. G.; Harrington, P. C. *Adv. Inorg. Biochem.* **1983**, *5*, 51–85.
(40) Muhoberac, B. B.; Wharton, D. C.; Babcock, L. M.; Harrington, P. C.; Wilkins, R. G. *Biochim. Biophys. Acta* **1980**, *626*, 337–345.
(41) Kurtz, D. M., Jr.; Sage, J. T.; Hendrich, M.; Debrunner, P. G.; Lukat, G. S. *J. Biol. Chem.* **1983**, *258*, 2115–2117.
(42) Mockler, G. M.; de Jersey, J.; Zerner, B.; O'Connor, C. J.; Sinn, E. *J. Am. Chem. Soc.* **1983**, *105*, 1891–1893.
(43) Stenkamp, R. E.; Sieker, L. C.; Jensen, L. H. *J. Am. Chem. Soc.* **1984**, *106*, 618–622. Stenkamp, R. E.; Sieker, L. C.; Jensen, L. H.; McCallum, J. D.; Sanders-Loehr, J. *Proc. Natl. Acad. Sci. U.S.A.* **1985**, *82*, 713–716.
(44) (a) Woodland, M. P.; Patil, D. S.; Cammack, R.; Dalton, H. *Biochim. Biophys. Acta* **1986**, *873*, 237–242. (b) Fox, B. G.; Surerus, K. K.; Münck, E.; Lipscomb, J. D. *J. Biol. Chem.* **1988**, *263*, 10553–10556.
(45) Day, E. P.; David, S. S.; Peterson, J.; Dunham, W. R.; Bonvoisin, J. J.; Sands, R. H.; Que, L., Jr. *J. Biol. Chem.*, in press.
(46) (a) Bancroft, G. M.; Maddock, A. G.; Randl, R. P. *J. Chem. Soc. A* **1968**, 2939–2944. (b) Cox, M.; Fitzsimmons, B. W.; Smith, A. W.; Larkworthy, L. F.; Rogers, K. A. *Chem. Commun.* **1969**, 183–184. (c) Buckley, A. N.; Wilson, G. V. H.; Murray, K. S. *Solid State Commun.* **1969**, *7*, 471–474. (d) Buckley, A. N.; Wilson, G. V. H.; Murray, K. S. *Chem. Commun.* **1969**, 718–719. (e) Buckley, A. N.; Rumbold, B. D.; Wilson, G. V. H.; Murray, K. S. *J. Chem. Soc. A* **1970**, 2298–2302. (f) Buckley, A. N.; Herbert, I. R.; Rumbold, B. D.; Wilson, G. V. H.; Murray, K. S. *J. Phys. Chem. Solids* **1970**, *31*, 1423–1434. (g) Torens, M. A.; Straub, D. K.; Epstein, L. M. *J. Am. Chem. Soc.* **1972**, *94*, 4160–4162. (h) Lang, G.; Boso, B.; Erler, B. S.; Reed, C. A. *J. Chem. Phys.* **1986**, *84*, 2998–3004.

**Scheme II**[a]

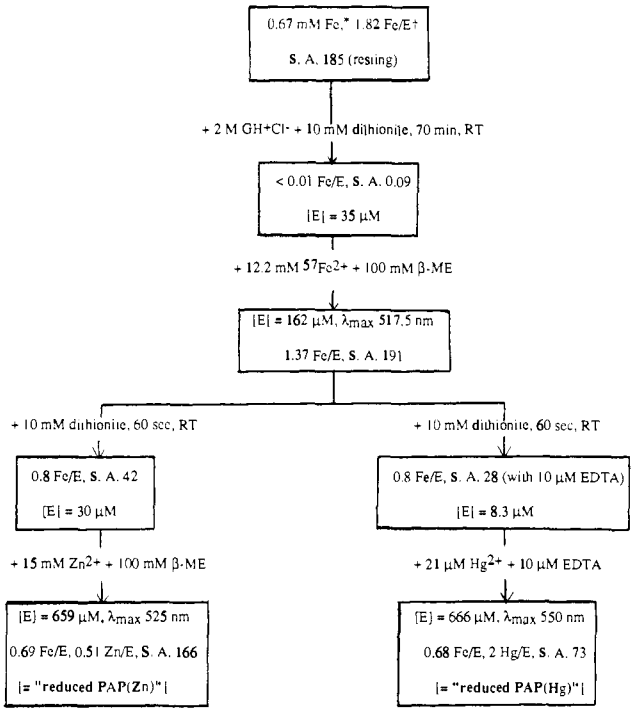


[a] Fe* denotes total iron concentration of enzyme sample. E† denotes two enzyme samples were combined.

important conclusions about the assignment of the two iron sites and about metal exchange can be drawn.

## Materials and Methods

PAP was purified from allantoic fluid collected from pregnant sows at the 65th day of gestation[32] as described previously.[13] Activity was determined at 25 °C in 0.1 M acetate buffer, pH 4.9, with *p*-nitrophenyl phosphate as substrate.[13] The enzyme concentration was estimated from the absorbance, assuming $A^{1\%}_{1cm}$ = 14.2 at 280 nm and a molecular mass of 40 kDa.[13] Metal concentrations were based on atomic absorption determined with a Varian AA-6 spectrometer.

The following procedure was used to obtain fully $^{57}$Fe-enriched, reduced PAP. Metal-free apoenzyme was prepared by mixing native enzyme (5 mL; 0.575 mM) in 0.1 M acetate buffer, pH 4.9, with guanidinium chloride ($GH^+Cl^-$, 10 mL; 3 M) in the same buffer and freshly prepared sodium dithionite (0.2 mL; 0.75 M). After 70 min at 25 °C the mixture was chromatographed on Sephadex G-25 (80.5 × 3.3 cm) in 0.1 M acetate buffer, pH 4.9. The apoenzyme (84 mL; 0.038 mM) had a specific activity (SA)[13] of 1.7 units/(mL $A_{280}$) as compared with 360 for active enzyme and contained 0.02 atom of Fe per molecule. To this apoenzyme were added 0.6 mL of neat β-mercaptoethanol (β-ME) and $^{57}FeCl_2$, giving final concentrations of 0.1 M and 8.6 mM, respectively. After 84 h at 25 °C, the solution had a specific activity of 350 units/(mL $A_{280}$). Concentration to 3 mL by ultrafiltration (Amicon PM 10 membrane) at 5 °C was followed by chromatography on Sephadex G-25 (40 × 2.3 cm), and the eluate was concentrated to 3 mL. The final sample had the following characteristics: Enzyme concentration, [E] = 0.63 mM; $A_{280}/A_{260}$ = 1.61; $A_{280}/A_{530}$ = 19.1; [Fe]/[E] = 1.64; specific activity = 260 units/(mL $A_{280}$); $\lambda_{max}$ = 510 nm. Most of this sample was frozen for storage and shipment; 1 mL was oxidized at 0 °C with 2.1 mM $H_2O_2$ for 10 min and subsequently chromatographed on Sephadex G-25. The eluate was concentrated to 1 mL and gave a sample with the following properties: [E] = 0.49 mM; $A_{280}/A_{260}$ = 1.58; $A_{280}/A_{530}$ = 19.4; [Fe]/[E] = 1.55; specific activity = 6.9 units/(mL $A_{280}$); $\lambda_{max}$ = 555 nm.

Unenriched enzyme for EPR studies was prepared similarly. Native protein (1.4 mL; 0.164 mM) in 0.1 M acetate buffer, pH 4.9, was treated with β-mercaptoethanol (10 μL; 90 mM final concentration) and $Fe^{2+}$ (0.2 mL; 38 mM) for 18 h at 25 °C, followed by Sephadex G-25 chromatography and concentration of the eluted enzyme. The characteristics of the resulting sample were as follows: [E] = 0.17 mM; $A_{280}/A_{260}$ = 1.56; $A_{280}/A_{530}$ = 14.7; [Fe]/[E] = 2.1; specific activity = 304 units/(mL $A_{280}$); $\lambda_{max}$ = 510 nm. Oxidized protein was prepared by reaction of native enzyme (1.4 mL; 0.145 mM) with $H_2O_2$ (0.1 mL; 2.4 mM final concentration) for 14 min at 0 °C followed by chromatography and concentration as above to give [E] = 0.308 mM, $A_{280}/A_{260}$ = 1.55, $A_{280}/A_{530}$ = 15.3, [Fe]/[E] = 1.9, specific activity = 21 units/(mL $A_{280}$), and $\lambda_{max}$ = 555 nm.

Schemes I and II summarize the modifications in these procedures that were used to prepare samples with differential $^{56}Fe/^{57}Fe$ enrichment and Zn- and Hg-substituted samples, respectively. If native enzyme is treated with dithionite, one of the two irons is lost rapidly to give a nominal $Fe_1$ species, whereas the second iron is lost more slowly. We refer to the partially enriched samples made by reconstitution of the $^{56}Fe_1$ species with $^{57}$Fe as "rapid $^{57}$Fe" or R and to the samples made from an $^{57}Fe_1$ species by reconstitution with $^{56}$Fe as "slow $^{57}$Fe" or S. The fully enriched material is labeled F wherever confusion with the partially enriched samples is possible. The label PAP(M) for the metal-substituted enzyme is self-explanatory.

Mössbauer data were recorded on an alternating constant-acceleration spectrometer. The minimum instrumental line width was Γ = 0.24 mm/s full width at half-maximum. The sample was maintained at constant temperature either in a Janis helium flow cryostat or in a superconducting magnet system of our construction. With the Janis cryostat small magnetic fields could be applied with permanent magnets either parallel or perpendicular to the γ-ray beam, or the field could be zeroed to B < 5 μT with the help of three orthogonal Helmholtz coils. Simple spectra were least squares fitted by a sum of Lorentzians,[47] while an iterative simulation technique was used to best reproduce the magnetically split spectra.[48] All isomer shifts are quoted relative to iron metal at 300 K.

A Bruker ER 200 X-band spectrometer with an Oxford ESR 9 helium flow cryostat was used for the EPR experiments. Spin quantifications were based on a CuEDTA standard. The reading of the temperature controller was calibrated against a carbon resistor thermometer immersed in a glycerol-filled EPR tube.

**Table I.** Mössbauer Parameters in mm/s for Fast-Fluctuation Spectra of Reduced PAP[a]

| $T$ (K) | $\Delta E_Q$(A) | $\delta_{Fe^A}$ | Γ(A) | $\Delta E_Q$(B) | $\delta_{Fe^B}$ | Γ(B) |
|---|---|---|---|---|---|---|
| 30 | 1.84 | 0.54 | 0.71 | 2.68 | 1.24 | 0.33 |
| 60 | 1.84 | 0.53 | 0.43 | 2.68 | 1.24 | 0.28 |
| 100 | 1.80 | 0.52 | 0.40 | 2.65 | 1.22 | 0.29 |
| 125 | 1.79 | 0.52 | 0.37 | 2.62 | 1.21 | 0.29 |
| 150 | 1.79 | 0.50 | 0.37 | 2.59 | 1.19 | 0.29 |
| 175 | 1.80 | 0.49 | 0.35 | 2.57 | 1.18 | 0.28 |
| 200 | 1.79 | 0.48 | 0.34 | 2.55 | 1.16 | 0.28 |
| 225 | 1.80 | 0.47 | 0.36 | 2.52 | 1.15 | 0.29 |

[a] Based on Lorentzian fits with pairwise equal areas and widths.

## Results and Discussion

At temperatures above 30 K the Mössbauer spectra of *reduced PAP* consist of two quadrupole doublets of roughly equal areas that can be assigned to a high-spin ferric site (A) and a high-spin ferrous site (B) on the basis of their isomer shifts, $\delta_{Fe}$, and their quadrupole splittings, $\Delta E_Q$. Table I lists the results of Lorentzian least-squares fits of data taken at different temperatures. The parameters of site B are typical of high-spin ferrous ions, but $\Delta E_Q \approx 1.83$ mm/s of site A is unusually large for a high-spin ferric ion with a nominal $^6A_1$ ground state. The line widths $\Gamma_A$ of the ferric site are systematically larger than those of the ferrous site, similar differences found in compounds with isolated high-spin iron ions have been explained in terms of a spin fluctuation model.

The spectra observed at 4.2 K in an applied field are fundamentally different as shown in Figure 1. In place of two quadrupole doublets we see a broad spectrum with several resolved features, which is indicative of magnetic hyperfine interactions at both iron sites. The overall splitting of ~11 mm/s implies internal fields $B^{int}$ in excess of 30 T but much less than the 55 T observed in most isolated high-spin ferric ions. Comparison of traces a and b in Figure 1 shows that the direction of an externally applied 32-mT field changes the spectra significantly. No differences in the 32-mT spectra were observed, however, on cooling the sample to 1.8 K. We draw two conclusions from these qualitative observations: (i) at 4.2 K the internal fields are stationary on the Mössbauer time scale, and (ii) since the internal

(47) Chrisman, B. L.; Tumolillo, T. A. *Comput. Phys. Commun.* **1971**, *2*, 322–330.
(48) Münck, E.; Groves, J. L.; Tumolillo, T. A.; Debrunner, P. G. *Comput. Phys. Commun.* **1973**, *5*, 225–238.

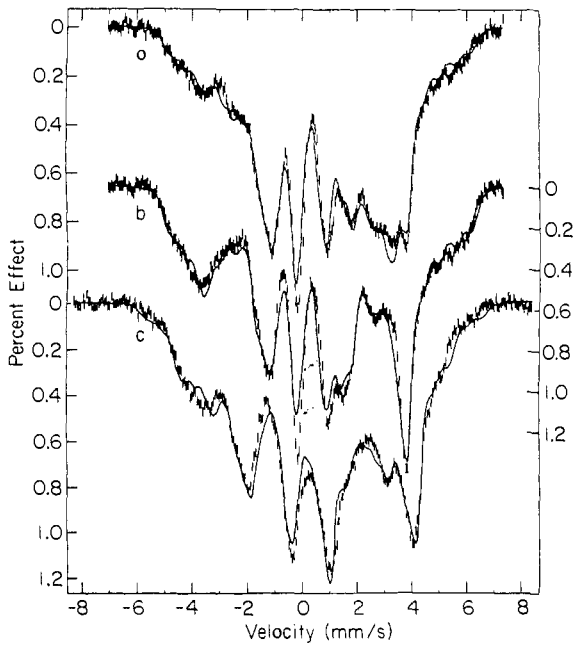


**Figure 1.** Mössbauer spectra of reduced PAP recorded at 4.2 K in magnetic fields of 32 mT (a) perpendicular and (b) parallel to the $\gamma$-ray beam and (c) in a 3.73-T field parallel to the $\gamma$-ray beam. The solid lines are simulations based on eq 1 using the parameters listed in Table II.

fields at both sites appear to follow the external field while being smaller than in isolated ions, they must result from spin coupling of the two iron sites to the effective spin $S = {}^1/_2$ observed by EPR. Under these conditions it should be possible to parametrize the Mössbauer spectra by the effective spin Hamiltonian

$$H = \beta \mathbf{S} g \mathbf{B} + \sum_i \mathbf{S} A_i \mathbf{I}_i + \sum_i \mathbf{I}_i P_i \mathbf{I}_i - \sum_i \beta_N g_N \mathbf{I}_i \mathbf{B}, \; i = A, B \qquad (1)$$

where $S = {}^1/_2$ is the effective spin of the ground Kramers doublet, $g$ is the effective $g$ tensor measured by EPR, and the second, third, and fourth terms represent the magnetic hyperfine, electric quadrupole, and nuclear Zeeman interactions of the two nuclei A and B, respectively. The quadrupole interaction vanishes in the ground state of $^{57}$Fe with nuclear spin $I = {}^1/_2$; in the $I = {}^3/_2$ excited state, it has the explicit expression $\mathbf{I}P\mathbf{I} = (eQV_{\zeta\zeta}/12)[3I_\zeta^2 - 15/4 + \eta(I_\xi^2 - I_\eta^2)]$, where $V_{\alpha\beta}$ is the negative of the electric-field gradient at the nucleus, $(\xi, \eta, \zeta)$ defines its principal axes, $V_{\zeta\zeta}$ is the component of largest magnitude, and $\eta$ is the asymmetry parameter $\eta = (V_{\xi\xi} - V_{\eta\eta})/V_{\zeta\zeta}$.

With the proper choice of the tensors $A_i$ and $P_i$ and the experimental $g$ values observed in EPR, eq 1 is expected to reproduce the low-temperature spectra. The quadrupole tensors $P_i$ must yield the splittings $\Delta E_Q = (eQV_{\zeta\zeta}/2)(1 + \eta^2/3)^{1/2}$, which can be extrapolated to 4.2 K from the measurements at higher temperatures in Table I. Thus only the signs of $V_{\zeta\zeta}$ for sites A and B, the asymmetries $\eta_i$, and the orientations of the tensors $P_i$ remain to be determined. For the hyperfine tensors $A_i$, on the other hand, only a rough estimate can be made on the basis of the overall splitting and the assumption of strong coupling, which was first invoked by Gibson et al. in the case of the 2Fe-2S proteins.[49] Equation 1 expresses the $^{57}$Fe hyperfine interactions in terms of the effective spin $\mathbf{S}$ rather than the intrinsic spins $\mathbf{S}_i$; it takes advantage of the Wigner–Eckart theorem,[50] which asserts that within the ground Kramers doublet the matrix elements of the operators $\mathbf{S}_A$ and $\mathbf{S}_B$ are proportional to those of $\mathbf{S}$. This proportionality assures the equivalence of the form $\mathbf{S}A_i\mathbf{I}_i$ in eq 1 for the $^{57}$Fe hyperfine interaction with the intrinsic forms $\mathbf{S}_i a_i \mathbf{I}_i$ for an (isolated) iron of electron spin $\mathbf{S}_i$ and nuclear spin $\mathbf{I}_i$. If the exchange interaction $H_{ex}$

$$H_{ex} = -2J\mathbf{S}_A\mathbf{S}_B \qquad (2)$$

is much larger than the zero-field splittings $H_{ZF}$

$$H_{ZF} = \sum_i \mathbf{S}_i D_i \mathbf{S}_i, \; i = A, B \qquad (3)$$

we may assume no mixing between different spin multiplets and use the relations[49]

$$\langle M'|S_A|M\rangle = (7/3)\langle M'|\mathbf{S}|M\rangle; \; \langle M'|\mathbf{S}_B|M\rangle = -(4/3)\langle M'|\mathbf{S}|M\rangle \qquad (4)$$

where the matrix elements are taken in the ground doublet, $S = {}^1/_2$. Corrections for the case where the interactions given by eq 2 and 3 are of comparable magnitude will be discussed later.

Since the (intrinsic) hyperfine coupling $a_A$ of high-spin ferric iron arises primarily from the Fermi contact term, it is expected to be isotropic, $a_A/(\beta_N g_N) \approx -22$ T, and the estimate $A_A/(\beta_N g_N) \approx -51$ T with a saturation field of $\mathbf{B}^{sat} = \mathbf{S}A_A/(\beta_N g_N) \approx -26$ T follows from eq 4. No prediction can be made at this point for $A_B/(\beta_N g_N)$ of the ferrous site other than that it is expected to be positive with an average of 29 T if orbital contributions are negligible. A search in parameter space starting with these estimates led to the values listed in Table II, which yield the simulations shown as solid lines in Figure 1. The differences between the spectra a–c in weak parallel and perpendicular fields and in strong parallel field, respectively, gave important clues in the choice of the parameters. As Figure 2 shows, the component spectrum arising from the ferrous site is concentrated between −2.5 and +4.5 mm/s; thus the outer wings of the spectra are entirely due to the ferric contribution. It is impossible to fit the left wing unless $A_A$ is chosen to be highly anisotropic. The uniqueness of the solution

**Table II.** Empirical Low-Temperature Mössbauer Parameters of Reduced PAP[a]

| | $Fe^{3+}$ | $Fe^{2+}$ |
|---|---|---|
| $g$ | (1.56, 1.72, 1.93) | |
| $\delta_{Fe}$ (mm/s) | 0.54 | 1.24 |
| $\Delta E_Q$ (mm/s)[a] | (−)1.85 | (+)2.68 |
| $\eta$ | 0 | 0.3 |
| $A/g_N\beta_N$ (T) | −(68, 45, 25) | +(26, 18, 10) |
| $R$(A→P)[b] | (60°, 60°, 0°) | (90°, 60°, 90°) |

[a] The sign of $V_{\zeta\zeta}$ (component of largest magnitude) is given in parentheses. [b] Euler angles[50] $(\alpha, \beta, \gamma)$ that rotate the A frame into the P frame.

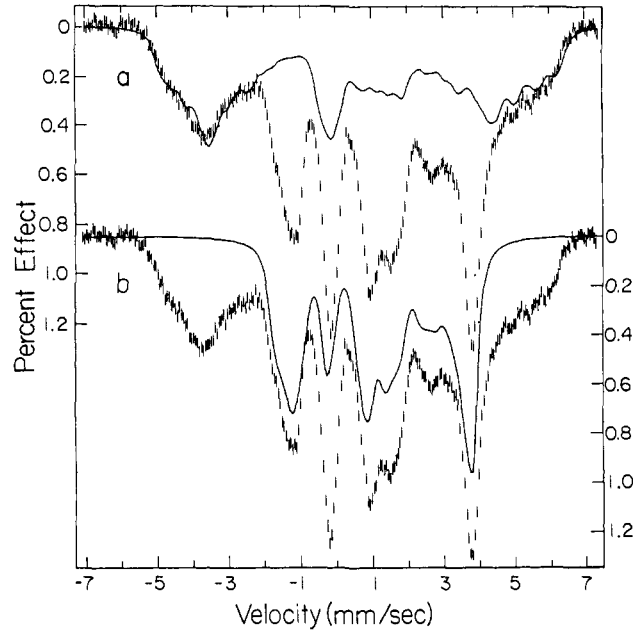


**Figure 2.** Spectrum of Figure 1b with simulations of (a) ferric and (b) ferrous contributions.

(49) Gibson, J. F.; Hall, D. O.; Thornley, J. H. M.; Whatley, F. R. *Proc. Natl. Acad. Sci. U.S.A.* **1966**, *56*, 877–879.
(50) For a definition see, e.g., Brink, D. M.; Satchler, G. R. *Angular Momentum*; Oxford University Press: Oxford, England, 1962.

**Table III.** Assumed Intrinsic Parameters of the Ground Doublet Sites A and B and Resulting Effective Parameters of the Ground Doublet Obtained from Equations 1-3, 5, and 6[a]

| | $Fe^{3+}$ | $Fe^{2+}$ |
|---|---|---|
| $a/(\beta_N g_N)$ (T) | −20 | −(18.8, 21.8, 12.3)[b] |
| $Tr(g)/3$ | 2 | 2.07 |
| $D$ ($cm^{-1}$) | −1.5 | −8 |
| $E$ ($cm^{-1}$) | −0.4 | −1.5 |
| **g** | (1.69, 1.93, 1.56)[c] | |
| $A_i/(\beta_N g_N)$ (T) | −(43.2, 27.9, 64.8)[c] | (24.1, 9.4, 28.0)[c] |

[a] Based on the values $-2J = 20$ $cm^{-1}$, $\lambda = -100$ $cm^{-1}$, $k = 0.8$, and an Euler angle[50] of $\beta = 90°$ between the principal axes of $D_A$ and $D_B$. The latter serves as reference frame for the components of **g** and $A_i$. [b] Based on eq 6. [c] Permutation of components yields **g** and $A_i$ tensors that approximate the empirical values in Table II.

and the uncertainty, $\Delta A_i$, of the parameters are difficult to judge, but a conservative estimate based on many simulations is $\Delta A_i/(\beta_N g_N) = \pm 3$ T. Because of the rather modest anisotropy of the **g** tensor, the simulations are insensitive to the relative orientation of $A_A$ and $A_B$ with respect to **g**, but the relative orientations of $A_i$ and $P_i$ are well defined. While eq 1 provides an adequate parametrization of the spectra in Figure 1, the parameters of Table II relating to the magnetic properties are clearly incompatible with the strong coupling model expressed by eq 4. The problem is most obvious for the phenomenological **A** tensor of the high-spin ferric site (A). Contrary to expectation, $A_A$ is highly anisotropic, although the intrinsic $a_A$ must be essentially a scalar as it derives primarily from the Fermi contact term. If we drop the assumption of strong coupling, however, the inconsistencies disappear. On a more fundamental level, then, we consider the Hamiltonian

$$H = H_{ex} + H_{ZF} + \beta\sum_i \mathbf{S}_i g_i \mathbf{B} + \sum_i \mathbf{S}_i a_i \mathbf{I}_i + \sum_i \mathbf{I}_i P_i \mathbf{I}_i - \sum_i \beta_N g_N \mathbf{I}_i \mathbf{B},\ i = \text{A, B} \quad (5)$$

using the definitions of $H_{ex}$ and $H_{ZF}$ given in eq 2 and 3, and we seek a solution with $g_A$ (=2) and $a_A$ both scalars. To reduce the number of free parameters we use second-order perturbation expressions[51] that relate $g_B$, $D_B$, $E_B$, and $a_B$:

$$g^B_{xx} = g^B_{zz} - (2k/\lambda)(D_B - E_B);\ g^B_{yy} = g^B_{zz} - (2k/\lambda)(D_B + E_B);\ a^B_{ij} = -P(\kappa\delta_{ij} + g_s\delta_{ij} - g^B_{ij}) \quad (6)$$

where we have ignored lesser terms in $a_B$[52] and introduced $P/(\beta_N g_N) \approx 63$ T and $\kappa \approx 0.35$; $g_s\delta_{ij} - g^B_{ij}$ is the deviation of the ferrous **g** tensor from the isotropic free-electron value $g_s \approx 2$. $D_B$ and $E_B$ are defined by the traceless, principal-axis form of the zero-field splitting, eq 3, $H_{ZF} = D_B(S^B_{z^2} - 2) + E_B(S^B_{x^2} - S^B_{y^2})$, the orbital reduction factor $k$ is taken as 0.8, and the spin-orbit coupling $\lambda$ as $-100$ $cm^{-1}$. The other relevant parameters were varied over the ranges $0 < |D_i| < 10$ $cm^{-1}$, $0 < (E_i/D_i) < (1/3)$, $2 < Tr(g_B)/3 < 2.5$, and 18 T $< -a_A/(g_N\beta_N) <$ 22 T. For simplicity, all tensors in eq 5 except for $P_i$ were assumed to have the same principal axes, but permutations of axes were allowed. The solution strongly depends on the ratio of the zero-field splitting to the exchange coupling. Adoption of this approach then allows us to estimate this ratio. With the value $-2J = 20$ $cm^{-1}$ estimated from NMR[21] and the parameters listed in Table III, the phenomenological tensors **g** and $A_i$ of eq 1 could be approximated as $g = (1.69, 1.93, 1.56)$, $A_A/(g_N\beta_N) = -(43.2, 27.9, 64.8)$ T, and $A_B/g_N\beta_N) = (24.1, 9.4, 28.0)$ T. A permutation of axes will bring the empirical parameter set of Table II into correspondence with the calculated set of Table III. The model predicts the next two Kramers doublets, which are part of an effective spin quartet, at 25 and 41 $cm^{-1}$. We note that the principal axes of the $D_A$ ($S = {}^5/_2$) were rotated by the Euler angles[50] (0°, 90°, 0°) from those of $D_B$ ($S = 2$) and that the calculated components of **g** and $A_i$ given above are referred to the principal axes defined by $D_B$.

Although the agreement with the empirical data given in Table II is not perfect, we feel that it is adequate to prove our point, given the limited experimental accuracy and the restricted parameter space explored.[53] We note that the coefficients $\lambda/k$, $P$, and $\kappa$ of eq 6 are frequently taken as adjustable rather than fixed as they are here and that in highly covalent compounds their values may be up to a factor of 2 smaller than the ones used here.[51] The adopted value[21] of the exchange coupling, $-2J = 20$ $cm^{-1}$, has been confirmed by susceptibility measurements.[45] The zero-field splittings found in this analysis are reasonable as they fall in the range observed in other five- or six-coordinate high-spin ferric and ferrous compounds.[54]

Additional evidence on the intrinsic Fe(III) parameters comes from EPR and Mössbauer measurements on *Zn- and Hg-substituted PAP*.[23] We first characterize the magnetic properties and the specific activity of the Fe(III)–M(II) samples and then argue that the Fe(III) has essentially the same environment and presumably the same ligands as the A site of the native enzyme; consequently, the Fe(III)–Zn/Hg derivative should allow one to study the A site unencumbered by the complexities of spin coupling.

All Zn- or Hg-substituted samples contained some native Fe(III)–Fe(II) enzyme, recognizable from the "$g \sim 1.72$" EPR signal and the broad, magnetically split low-temperature Mössbauer spectra. The EPR showed, in addition, strong signals near $g \sim 4.3$ characteristic of the second Kramers doublet of high-spin ferric iron in a low-symmetry environment. The corresponding weaker ground-state signal was observed near $g \sim 9.4$. The "$g \sim 4.3$" signal could arise (i) from binuclear Fe(III)–M(II) clusters, (ii) from molecules having a single site occupied by an Fe(III) and the other site empty, and (iii) from adventitious iron. In native and $^{57}$Fe-enriched samples prepared by similar procedures the "$g \sim 4.3$" signal accounted for less than 3% of the total iron present, and there is little reason to assume a larger percentage of single-site and/or adventitious iron in the Zn- and Hg-substituted protein. The bulk of the "$g \sim 4.3$" signal in the latter can then be ascribed to the Fe(III)–M(II) clusters, presumably A-site Fe(III) since the samples were prepared under reducing conditions. Double integration of the EPR derivative yielded the spin or, equivalently, the iron concentrations listed in Table IV. Taking the maximum specific activity of native enzyme to be $SA_{max} = 387$ units/(mL $A_{280}$), the concentrations of the "$g \sim 1.72$" species in column 6 imply the specific activities listed in column 9, and the differences between the measured values in column 8 and the calculated values in column 9 then represent the specific activities of the mixed-metal clusters as given in the last column. The results of Table IV suggest that PAP(Zn) has about half the activity of the native enzyme, while PAP(Hg) has only marginal activity. Considering the experimental errors involved in obtaining these specific activities, they are in reasonable agreement with the estimates made earlier by more direct measurements.[23]

Since the Mössbauer spectra of the PAP(Zn) and PAP(Hg) samples were complex and of low intensity, we did not analyze them quantitatively. The iron corresponding to the "$g \sim 4.3$" site, however, could easily be identified in the 4.2 K spectra as a six-line pattern with an overall splitting of ~17 mm/s equivalent to an internal field $B^{int} \approx 53$ T. Given the hyperfine coupling of high-spin Fe(III) discussed earlier, $a/(g_N\beta_N) \approx -22$ T, such a large internal field implies a spin expectation value $\langle S \rangle \approx {}^5/_2$ and is characteristic of the ground state of a spin $S = {}^5/_2$ with zero-field splitting $H_{ZF} = D(S^2_z - S^2/3) + E(S^2_x - S^2_y)$ in the limit $E/D \approx$

(51) Abragam, A.; Bleaney, B. *Electron Paramagnetic Resonance of Transition Ions*; Oxford University Press: Oxford, England, 1970; eq 19.32, 19.33.

(52) To avoid the introduction of additional parameters, we ignore the traceless spin dipolar contribution to $a_B$, $P\langle l_{pq}\rangle_m/14$ in the notation of ref 51, although its components may be of comparable magnitude as those of the orbital term, $P(g_{ij} - g_s\delta_{ij})$ in eq 6. While eq 19.32 and 19.33 of reference 51 suggest that $l_{pq}$ can be deduced from the electric quadrupole interaction, this is not the case here since $\langle l_{pq}\rangle_s$ in the 3d valence contribution to $P_B$ of eq 1 is the matrix element over all occupied 3d orbitals, whereas $\langle l_{pq}\rangle_m$ is taken over the unpaired electrons only. Moreover, the experimental $P_B$ contains unknown nonvalence contributions that may be of the order of $P_A$.

(53) $g_B$, $D_B$, $E_B$, and $a_B$ were not constrained by eq 6 in the solution reported earlier.[38]

(54) Reem, R. C.; Solomon, E. I. *J. Am. Chem. Soc.* **1984**, *106*, 8323–8325.

**Table IV.** Chemical and EPR Data on Zn- and Hg-Substituted PAP[a]

| sample | [E] | [Fe] | [M] | $[Fe_{4.3}]^b$ | $[Fe_{1.72}]^c$ | $[Fe_{EPR}]^d$ | SA | $SA_{1.72}{}^e$ | $SA_{MFe(III)}{}^f$ |
|---|---|---|---|---|---|---|---|---|---|
| PAP(Zn) | 250 | 210 | 190 | 145 | 2 × 25 | 195 (15) | 254 | 39 | 215 |
| PAP(Hg) | 550 | 630 | 870 | 140 | 2 × 170 | 480 (50) | 135 | 119 | 16 |

[a] Concentrations in μM. [b] Concentration of the site(s) giving rise to the $g \approx 4.3$ EPR signal assuming a fractional population of 1/3 in the second Kramers doublets of the spin sextet. [c] Iron concentration in the native Fe(III)–Fe(II) cluster based on the intensity of the $g$ = (1.56, 1.72, 1.93) signal. [d] Total concentration of EPR-active iron; sum of columns 5 and 6. Numbers in parentheses are estimated uncertainties in units of the least significant digit. [e] Specific activity in units/(mL $A_{280}$) due to native enzyme present; $SA_{1.72} = SA_{max}[Fe_{1.72}]/(2[E])$; $SA_{max}$ = 387. [f] Specific activity assignable to binuclear mixed-metal clusters; difference between columns 8 and 9.

1/3. While the two innermost lines of the six-line spectrum were covered by other spectral components, lines 1, 2, 5, and 6 were reasonably well resolved. As a consequence, it was possible to determine the quadrupole interaction along the internal field as reflected in the difference between the splittings of the outer two pairs of lines. If the six-line pattern (and the "$g \sim 4.3$" EPR signal) indeed arises from A-site Fe(III), and if our earlier analysis of the coupled system is correct, then the intrinsic parameters of the A site listed in Table III should reproduce the observed six-line spectrum. We found that this was indeed the case with a slight adjustment of the Euler angle[50] $\beta$ from 60° (Table II) to 67° and of the intrinsic hyperfine coupling $a/(g_N\beta_N)$, from −20 T (Table III) to −21 T. Moreover, the rhombicity, $E/D \approx 1/3$, implied by the "$g \sim 4.3$" signal, is not far from the value adopted for the A site, $E/D = 0.27$ in Table III. These differences are within the estimated experimental uncertainties. The good agreement is hardly a coincidence; it corroborates our model and suggests that the intrinsic properties of the A site are not noticeably affected by the (divalent) metal at the B site. If this conjecture is valid, the A site must have the same coordination in all Fe(III)–Mn(II) derivatives, and it should be possible to estimate $D_A$ directly from EPR.

In addition to the spectral components already mentioned, a quadrupole doublet due to high-spin ferrous iron was discernible at all temperatures; its quadrupole splitting, $\Delta E_Q = 2.68$ mm/s, and isomer shift, $\delta_{Fe} = 1.27$ mm/s at 4.2 K, match those of the B site in the reduced enzyme quite closely, suggesting that it arises from $^{57}$Fe(II) in a B site with an A site that is either empty or occupied by a diamagnetic ion. So far no information is available on $g_B$, $A_B$, $D_B$, and $E_B$ of the "isolated", not spin-coupled Fe(II) to check the agreement with the intrinsic parameters derived for the B site in Table III. In principle, these parameters could be deduced from high-field Mössbauer data. The mixed-metal preparations analyzed so far have not been sufficiently homogeneous and concentrated, however, to allow such detailed measurements.

All available evidence, then, supports the model of intermediate coupling for native PAP; i.e., the intrinsic zero-field splittings of the two sites are comparable to the exchange interaction, the effective **g** and **A** tensors of the coupled system deviate substantially from the predictions of the strong coupling model, eq 4, and we have to resort to the more complex Hamiltonian, eq 5.

Although the evaluation of eq 5 by computer is straightforward, it is desirable to have explicit expressions for the **g** and **A** tensors of the coupled system in terms of the intrinsic parameters of the two sites and the exchange interaction. Using eigenstates of $H_{ex}$, eq 2, and treating $H_{ZF} = \sum_i \mathbf{S}_i D_i \mathbf{S}_i$, $i$ = A, B, as a perturbation, we find to first order in $D/J$

$$\mathbf{g} = c_A g_A + c_B g_B + (1/5)c_A c_B(g_A - g_B)(b_A D_A - b_B D_B)/J \quad (7)$$

$$A_A = c_A a_A + (1/5)c_A c_B a_A(b_A D_A - b_B D_B)/J \quad (8a)$$

$$A_B = c_B a_B - (1/5)c_A c_B a_B(b_A D_A - b_B D_B)/J \quad (8b)$$

Here, $g_i$, $A_i$, $a_i$, and $D_i$ are 3 × 3 matrices, while $b_i$ and $c_i$ are numbers defined as follows:

$$b_i = 3c_i + 1 \quad (9a)$$

$$c_A = [S(S+1) + S_A(S_A+1) - S_B(S_B+1)]/[2S(S+1)] \quad (9b)$$

$$c_B = [S(S+1) + S_B(S_B+1) - S_A(S_A+1)]/[2S(S+1)] \quad (9c)$$

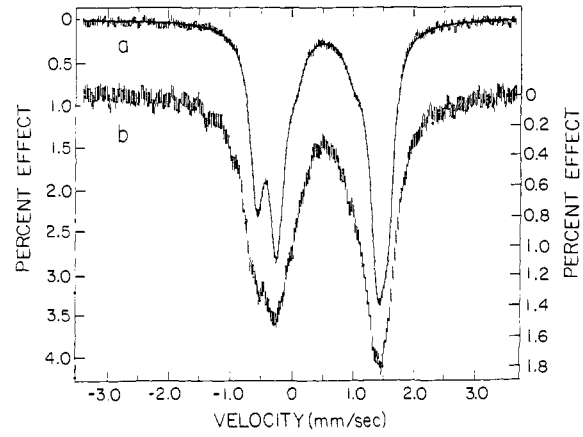


**Figure 3.** Mössbauer spectra of oxidized PAP recorded in a magnetic field of less than 5 μT (a) at 4.2 K and (b) at 119 K. The solid line in (a) represents a Lorentzian fit with three doublets as described in the text. In (b) contributions due to reduced PAP and the phosphate complex of oxidized PAP, comprising 11.4% and 8.8% of the total area, respectively, have been subtracted.

The calculation follows Scaringe et al.;[55] it applies to the $S = {}^1/_2$ ground doublet of any antiferromagnetically coupled system of spins $S_A = S_B + {}^1/_2$ and is valid for arbitrary orientations of the tensors $D_i$, $g_i$, and $a_i$, with the understanding that the physically meaningful quantities are $g^T\mathbf{g}$ etc.,[56] where $g^T$ is the transpose of **g**. The first terms of eq 7 and 8 are the usual strong-coupling limits;[49,55] the correction terms are typically small for **g** because of the factor $(g_A - g_B)$ but quite substantial for $A_i$ even for moderate $D/J$ ratios. The same conclusion was reached by Valentine,[56] who gave similar expressions for **g** and $A_i$ in the effective-spin ${}^1/_2$ ground state of an Fe(III)–Fe(II) complex; he noted that finite values of $D/J$ may also contribute to the anisotropy of up to 13% observed in the **A** tensor of the ferric site in reduced 2Fe-2S proteins.[57,58] Guigliarelli et al.[59] have recently used a more restricted model to estimate the anisotropy of the effective **g** tensor due to finite $D/J$ and corrected their earlier assumption[60] of strong coupling. They confirm that realistic estimates for $D$ and $J$ can explain the large spread in the **g** values and the low average **g** of PAP. These authors have not considered the **A** tensors, which are more critical and informative, and it

(55) Scaringe, R. P.; Hodgson, D. J.; Hatfield, W. E. *Mol. Phys.* **1978**, *35*, 701–713.

(56) Valentine, M. *Hyperfine Interact.* **1986**, *30*, 309–335.

(57) (a) Debrunner, P. G.; Münck, E.; Que, L.; Schulz, C. E. In *Iron-Sulfur Proteins*; Lovenberg, W., Ed.; Academic Press: New York, 1977; Vol. III, p 381. (b) Münck, E.; Debrunner, P. G.; Tsibris, J. C. M.; Gunsalus, I. C. *Biochemistry* **1972**, *11*, 855–863.

(58) In reduced putidaredoxin, specifically, the intrinsic **A** tensor of the high-spin ferric site is $a/(\beta_N G_N)$ = (17.4, 15.5, 13.3) T, assuming the strong coupling limit,[57b] whereas Fe(III) in the mononuclear iron-sulfur protein rubredoxin has an **A** tensor of $\mathbf{A}/(\beta_N g_N) = -(16.4, 15.6, 17.0)$ T.[57a] The larger anisotropy of the former can be accounted for by the second term of eq 8a. An order-of-magnitude estimate yields $-2J \sim 100$ cm$^{-1}$ assuming the A and B sites putidaredoxin have zero-field splittings comparable to those of the Fe(III) and Fe(II) states of rubredoxin and that $A(Fe^{III})$ of rubredoxin[57a] can be substituted for $a_A$ of putidaredoxin.

(59) Guigliarelli, B.; Bertrand, P.; Gayda, J.-P. *J. Chem. Phys.* **1986**, *85*, 1689–1692.

(60) Bertrand, P.; Guigliarelli, B.; Gayda, J.-P. *Arch. Biochem. Biophys.* **1986**, *245*, 305–307.

**Table V.** Temperature Dependence of the Effective Line Width $\Gamma^{eff}$ and Other Parameters of the Phosphate Complex of Oxidized PAP[a]

| $T$ (K) | 4.2 | 25 | 50 | 75 | 100 | 125 | 150 | 175 | 200 |
|---|---|---|---|---|---|---|---|---|---|
| $\Gamma^{eff}$ | 0.26 (1) | 0.26 (1) | 0.27 (1) | 0.30 (1) | 0.37 (2) | 0.44 (2) | 0.46 (2) | 0.41 (3) | 0.43 (4) |
| $\Delta E_Q$ | 1.39 (1) | 1.38 (1) | 1.36 (1) | 1.38 (1) | 1.34 (2) | 1.35 (3) | 1.34 (3) | 1.38 (3) | 1.40 (3) |
| $\delta_{Fe}$ | 0.54 (1) | 0.53 (1) | 0.53 (1) | 0.53 (1) | 0.52 (2) | 0.52 (3) | 0.51 (3) | 0.50 (3) | 0.51 (3) |
| $\Gamma^{eff}$ | 0.28 (1) | 0.28 (1) | 0.29 (1) | 0.32 (1) | 0.32 (2) | 0.39 (4) | 0.40 (3) | 0.45 (3) | 0.52 (3) |
| $\Delta E_Q$ | 1.04 (1) | 1.00 (1) | 0.99 (1) | 0.99 (1) | 0.95 (2) | 0.94 (4) | 0.95 (3) | 1.00 (4) | 1.04 (4) |
| $\delta_{Fe}$ | 0.52 (1) | 0.50 (1) | 0.50 (1) | 0.50 (1) | 0.49 (2) | 0.48 (4) | 0.46 (3) | 0.45 (4) | 0.44 (4) |

[a] Results in mm/s of least-squares fits by two Lorentzians with equal widths and areas for a given quadrupole pair. Numbers in parentheses are uncertainties in units of the least significant digit.

remains questionable whether their limited basis set can explain the experimental data.

As a final point we mention that several spin-coupled Fe(II-I)–Fe(II) complexes have been synthesized recently to mimic the active site of reduced PAP and related two-iron proteins.[61-63] Thus far, their Mössbauer spectra have not been analyzed in adequate detail to bear on the proposed spin-coupling model.

In contrast to the native enzyme, *oxidized PAP* exhibits no sign of magnetic hyperfine splitting of 4.2 K as is evident from the Mössbauer spectrum of Figure 3a. Earlier, we interpreted this and similar spectra as a superposition of two major quadrupole doublets arising from the two iron sites of oxidized PAP and an admixture of unknown origin.[22] More careful scrutiny of this and other samples[28] at different temperatures and fields revealed that the spectrum of Figure 3a contains two minority spectra, which can now be assigned quantitatively on the basis of the following observations.

For $T > 30$ K an isolated line appears near 2.6 mm/s, which accounts for slightly less than 3% of the total area of the spectrum in Figure 3a and matches the position of the outermost line in reduced PAP in the fast-spin fluctuation limit at corresponding temperatures. The three additional lines of reduced PAP overlap the major doublets, and the spectral admixture of reduced enzyme accounts for 11.4% of the original area of Figure 3a. At 4.2 K the spectrum of this component is broadened magnetically and extends from −11 to +10 mm/s in zero field: thus it does not contribute any noticeable features to Figure 3a. After subtraction of this component, the shoulders near 0 and 1 mm/s still remain; they can be assigned to the phosphate complex of oxidized PAP, whose Mössbauer parameters were recently reported.[28] Phosphate binds very tightly to oxidized PAP,[16] and the resulting complex exhibits a pair of quadrupole doublets with $\Delta E_Q(\delta_{Fe})$ in mm/s of 1.02 (0.52) and 1.38 (0.55) at 4.2 K, respectively.[28] We adjusted the subtracted area of this spectral component according to the criterion that the corrected spectrum should be fitted with minimum $\chi^2$ by two pairs of Lorentzians; we found that 8.8% of the original area, Figure 3a, was due to the phosphate complex of oxidized PAP.

The final parameters $\Delta E_Q(\delta_{Fe})$ in mm/s of the major doublets are 1.69 (0.55) and 2.17 (0.48); they differ little from the values reported earlier,[22] but within experimental uncertainty, the four lines now have equal areas and reasonable widths. The isomer shifts leave no doubt that both sites are high-spin ferric; although the quadrupole splittings are unusually large, they are comparable to the value found for the ferric site A of the reduced enzyme. The alternate pairing of lines to that given above leads to unreasonable isomer shifts and can therefore be ruled out.

The lack of magnetic hyperfine splitting in the low-temperature spectra of high-spin ferric ions is strong evidence for magnetic coupling to an integer spin system. More specifically, the Mössbauer data are compatible with a diamagnetic ground state of oxidized PAP as suggested by susceptibility measurements.[20,21,26]

At higher temperatures the spectra broaden unexpectedly as illustrated in Figure 3b for $T = 119$ K. This trace represents the "true" spectrum of oxidized PAP as the contributions from the

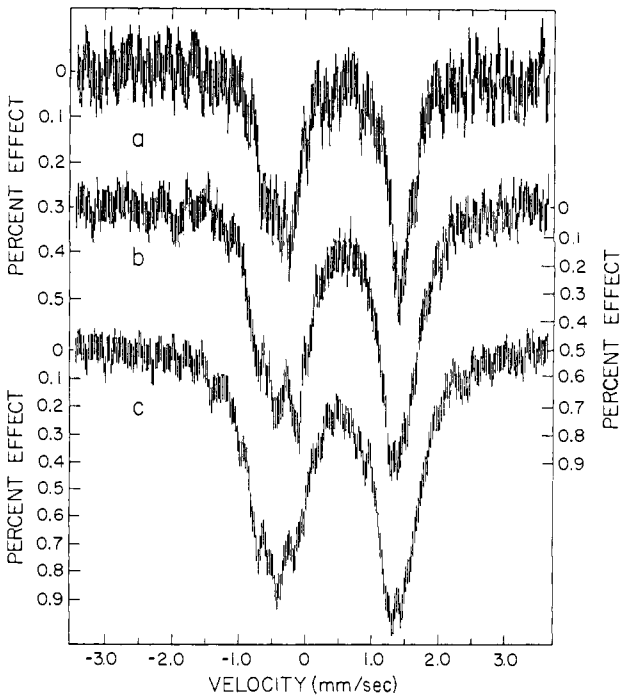


**Figure 4.** Mössbauer spectra of oxidized PAP after subtraction of a fraction $f(T)$ of the 4.2 K spectrum, Figure 3a, as recorded in a magnetic field of less than 5 $\mu$T. The temperatures and fractional areas $f$ were $T = 29.5$ K, $f = 83.4\%$ in (a), $T = 60.5$ K, $f = 55.6\%$ in (b), and $T = 119$ K, $f = 39.5\%$ in (c), respectively, corresponding to a triplet state at 80 K and a quintet at 240 K.

admixtures of reduced PAP and the phosphate complex of oxidized PAP have been subtracted. A four-line fit of Figure 3b leads to line widths $\Gamma$ of 0.49 mm/s as compared to 0.26 mm/s of the corrected 4.2 K spectrum. We noted this broadening with increasing temperature before and found that the spectral shape varies with the strength and direction of an applied field, suggestive of magnetic hyperfine interaction.[22] Similar, though less drastic thermal broadening is observed in the phosphate complex of oxidized PAP; attempts to fit the spectra by two pairs of Lorentzians of adjustable width $\Gamma(T)$ lead to the values listed in Table V. Here we show that the spectra of oxidized PAP broaden spontaneously even in a very small field of <5 $\mu$T, and we test the hypothesis that the effect arises from the thermal population of intrinsically broadened excited multiplets. The cause of this broadening is not yet understood as will be discussed later.

Since the singlet ground state populated at 4.2 K gives rise to narrow lines (Figure 3a), it is plausible to assume that the broadening arises from the population of excited spin states at higher temperatures. We can then ask whether the spectra can be explained as a superposition of an intrinsically narrow singlet spectrum and an intrinsically broad triplet spectrum, whereby the temperature dependence is given entirely by the Boltzmann factor. An attempt to test this hypothesis and to determine the energy $k\Delta(=-2J)$ of the triplet state is shown in Figure 4. To obtain these spectra the raw data were corrected for the 11.4% admixture of reduced PAP and 8.8% admixture of the oxidized phosphate complex, and a fraction $f(T) = 1/[1 + 3\exp(-\Delta/T) + 5\exp(-3\Delta/T)]$ of the corrected 4.2 K spectrum was subsequently

(61) Chaudhuri, P.; Winter, M.; Küppers, H.-J.; Wieghardt, K.; Nuber, B.; Weiss, J. *Inorg. Chem.* **1987**, *26*, 3302–3310.
(62) Borovik, A. S.; Murch, B. P.; Que, L., Jr.; Papaefthymiou, V.; Münck, E. *J. Am. Chem. Soc.* **1987**, *109*, 7190–7191.
(63) Borovik, A. S.; Que, L., Jr. *J. Am. Chem. Soc.* **1988**, *110*, 2345–2347.

**Table VI.** Mössbauer Parameters of Fully (F) and Partially Enriched (R, S) PAP and Its Phosphate Complexes[a]

| sample | $T$ (K) | site | $\Delta E_Q$[b] | $\delta_{Fe}$[b] | $\Gamma$[b] | $F_A$(F)[c] | $F_A$(R)[c] | $F_A$(S)[c] |
|---|---|---|---|---|---|---|---|---|
| reduced | 100 | A | 1.81 (2) | 0.52 (1) | 0.37 (3) | 50.0 (6) | 55 (3) | 45 (4) |
| | | B | 2.65 (2) | 1.22 (1) | 0.30 (2) | | | |
| reduced $P_i$[d] | 100 | A | 0.76 (3) | 0.54 (1) | 0.34 (2) | 49.6 (5)[e] | 53 (4) | 38 (6) |
| | | B | 2.75 (2) | 1.22 (2) | 0.34 (2) | | | |
| oxidized | 4.2 | A | 1.69 (1) | 0.55 (1) | 0.25 (1) | 50.5 (10) | 53 (3) | 45 (5) |
| | | B | 2.17 (2) | 0.48 (1) | 0.27 (1) | | | |
| oxidized $P_i$[d] | 4.2 | A | 1.39 (1) | 0.54 (1) | 0.27 (1) | 50.6 (9)[e] | 53 (2) | 41 (5) |
| | | B | 1.04 (1) | 0.52 (1) | 0.27 (1) | | | |

[a] Numbers in parentheses are estimated uncertainties in units of the least significant digit. [b] In units of mm/s. [c] Fractional areas of site A in percent of (corrected) total area for full (F), "rapid" (R), and "slow" (S) enrichment as explained under Materials and Methods. [d] Reduced $P_i$ and oxidized $P_i$ refer to the phosphate complexes of the reduced and oxidized forms of the enzyme, respectively. [e] Quoted from Pyrz, J. W.; Sage, J. T.; Debrunner, P. G.; Que, L., Jr. *J. Biol. Chem.* **1986**, *261*, 11015–11020.

subtracted. As Figure 4 shows, the criterion that the residual "triplet" spectra should be invariant can be approximately satisfied if $\Delta$ is chosen in the range of 80 ± 20 K. The limited accuracy of the data precludes a more detailed analysis, but we believe that the hypothesis of a thermally populated higher multiplet near 80 K is borne out.

Even for a higher multiplet, the broadening of the Mössbauer lines is puzzling, since the system has integral spin and thus is expected to have a vanishing spin expectation value in zero field. As a consequence, the magnetic hyperfine interaction, $(\mathbf{S}_i\mathbf{A}_i\mathbf{I}_i)$, is expected to vanish as well. This point was apparently missed by earlier workers who had observed thermal line broadening in other spin-coupled Fe(III)–Fe(III) dimers and had attributed it to spin relaxation effects in the high-spin states.[46a-g] The temperature and field dependences of the broadening in oxidized PAP indeed suggest a magnetic effect in the thermally populated triplet state. In the limit of zero applied field, however, time reversal symmetry holds, and any nondegenerate level of an integer spin system has a vanishing spin expectation value. An external magnetic field or the coupling to a nearby Kramers system can lift this restriction to the extent that the magnetic interaction mixes the zero-field eigenstates of comparable energies. The residual field $B < 5$ $\mu$T of the present experiment can induce a sizable spin expectation value only if the splitting of the zero-field states is of the order of $\Delta E < 10\ \mathbf{g}\beta B \sim 4 \times 10^{-5}$ cm$^{-1}$. The Kramers system most likely to couple to the electron spin is the $^{57}$Fe nucleus itself, producing the rarely observed pseudoquadrupole interaction. This second-order effect, given by the expression $\sum_{m\neq n}|\langle n|\mathbf{SAI}|m\rangle|^2/(E_n-E_m) = \mathbf{I}Q_n\mathbf{I}$, gives rise to a quadrupole tensor that varies with the electronic state.[64] If we conservatively estimate that a ±0.1 mm/s variation of the effective quadrupole splitting is sufficient to produce the broadening seen in Figure 4a, an energy splitting of at most 0.06 cm$^{-1}$ would be required in the triplet, which appears very unlikely. The effects of other nearby nuclei should be smaller still. Apart from the assumption of accidental near degeneracies in the excited spin multiplets, then, we can propose no reasonable explanation for the broadening.

Lang and co-workers recently reported analogous thermal line broadening in integer spin complexes of high-spin ferric iron with a tetraphenylporphyrin cation radical.[46h] To the extent that the zero-field splitting of the iron is axial, the sublevels $|M_S| = 1$, 2, and 3 of the ground multiplet are degenerate in zero field. The $^{57}$Fe hyperfine coupling will lift the degeneracy, and the system states have finite spin expectation values for the iron. In contrast to the case of Fe(III) tetraphenylporphyrin, there is no reason to assume an axial zero-field splitting in PAP. Thermal line broadening of integer spin complexes[46a-h] is obviously not a peculiarity of PAP, and more work is needed to resolve this question.

Up to this point there is no indication which of the two ferric sites of oxidized PAP derives from the ferric site (A) of the reduced enzyme. To answer this question, we next turn to the *partially enriched samples R and S*, which are expected to have Mössbauer spectra with larger and smaller contributions from site A than the fully enriched samples (F), respectively. The results for the reduced sample and its phosphate complex listed in Table VI verify these expectations. Although the differential enrichments of the samples R and S are small, they allow an unambiguous assignment of the quadrupole doublets seen in the Mössbauer spectra to the sites A and B of the enzyme. Hence, site A must be the site with the larger contribution in the samples R and vice versa, i.e., the site with quadrupole splitting $\Delta E_Q = 1.69$ and 1.39 mm/s in the oxidized sample and its phosphate complex, respectively.

The magnetic and Mössbauer properties of PAP are strikingly similar to those of the functionally unrelated binuclear iron protein hemerythrin,[39] an $O_2$-carrier of known structure[43] found in marine invertebrates. Oxidized PAP is analogous to the Fe(III)/Fe(III) met form, in which the two irons are linked by a $\mu$-oxo and two carboxylate bridges and have exchange interactions $-2J \approx 268$ cm$^{-1}$. Reduced PAP, on the other hand, is analogous to the Fe(III)/Fe(II) semimet forms of hemerythrin.[40,41] The latter have smaller exchange interactions and **g** tensors ranging from (1.96, 1.88, 1.67) to (1.87, 1.71, 1.40), which can be rationalized by the full Hamiltonian, eq 5, with the same model as we adopted here. A methane monooxygenase[44] with $g = (1.78, 1.88, 1.95)$ may contain a similar binuclear iron cluster. The **A** tensors, similarly, can be explained only if the zero-field splitting is taken into account together with the exchange interaction.[38] All these complexes as well as the $\mu$-oxo-bridged Fe(III)–Fe(III) cluster in ribonucleotide reductase[65] and hemerythrin model compounds[61-63,66] have unusually large quadrupole splittings of the ferric site(s). There is speculation, therefore, that PAP might have a $\mu$-oxo or $\mu$-hydroxo bridge as well,[31] but definite proof is still lacking.

While it is impossible to deduce the nature of the iron ligands from the Mössbauer data, there are, nevertheless, some general and some more speculative conclusions that may be drawn. (i) The isomer shift $\delta_{Fe}$ of the Fe(II) is larger than that of deoxyhemerythrin and model compounds with $FeN_3O_3$ coordination, suggesting only one or two nitrogenous ligands,[41,66] one of which has been identified as histidine.[21] (ii) The simulations of the spectra in Figure 1 required a rotation of the electric field gradients with respect to the common principal axes of **g**, $D_i$, and $\mathbf{A}_i$. To the extent that $\Delta E_Q$ of the ferrous site is dominated by contributions from the valence electrons, it follows from standard crystal field arguments that the local symmetry at the Fe(II) must be very low. [The symmetry at the Fe(III) is not likely to be higher, but the crystal field model fails to explain $\Delta E_Q$ of a $^6A_1$ state.] (iii) The anomalously large quadrupole splittings of the high-spin ferric iron in PAP, hemerythrin, ribonucleotide reductase, and model compounds remain to be explained quantitatively. For PAP all but the largest value, $\Delta E_Q = 2.17$ mm/s, have been matched in model compounds, and any attempt to rationalize the large splittings should focus on the well-characterized analogues.[61-63,66]

Finally, we comment on our attempts to enrich PAP differentially in $^{57}$Fe and to prepare mixed-metal clusters. Comparison of the preparation of "rapidly" (R) and "slowly" (S) enriched samples, as summarized in Scheme I, with the results given in

(64) Clauser, M. J.; Mössbauer, R. L. *Phys. Rev.* **1969**, *178*, 559–567.

(65) Petersson, L.; Gräslund, A.; Ehrenberg, A.; Sjöberg, B.-M.; Reichard, P. *J. Biol. Chem.* **1980**, *255*, 6706–6712. Atkin, C. L.; Thelander, L.; Reichard, P.; Lang, G. *J. Biol. Chem.* **1973**, *248*, 7464–7472.

(66) Hartman, J. A.; Rardin, R. L.; Chaudhuri, P.; Pohl, K.; Wieghardt, K.; Nuber, B.; Weiss, J.; Papaefthymiou, G. C.; Frankel, R. B.; Lippard, S. J. *J. Am. Chem. Soc.* **1987**, *109*, 7387–7396.

Table VI leads to the following conclusions. (i) Short treatment of PAP with dithionite removed preferentially site A iron, which is high-spin ferric in both stable states of the enzyme. Addition of $^{57}$Fe(II) restored activity, but $^{57}$Fe entered both A and B sites in a 53% to 47% ratio. Somewhat larger enrichment, 42% to 58%, was observed when a totally enriched $^{57}$Fe sample was treated with dithionite and then reconstituted with $^{56}$Fe(II).[67] In both cases, therefore, the added Fe(II) entered the A as well as the B sites, the former necessarily with a change in oxidation state; in other words, both sites had to be at least transiently unoccupied. Naively, one might have expected the short dithionite treatment to remove the A-site iron only, leaving the B-site iron intact. It appears, however, that the occupation of the two binding sites is in a dynamic equilibrium with so far unknown parameters. We do know that the "one-iron" enzyme is only slowly activated, and especially is this so in the presence of 2-mercaptoethanol.[15] It seems clear, therefore, that ligand exchange of the incoming Fe(II) [with enzyme-bound Fe(II)] occurs on a time scale fast compared to that of the oxidation leading to the active enzyme. It would be consistent with the data if the center indeed contained a $\mu$-hydroxo bridge, since the $\mu$-hydroxo form [Fe(II)–OH–Fe(II)] would be a likely species to be oxidized in the activation of the enzyme.

The only samples to show uncoupled high-spin Fe(II) with the parameters of the B site were the Zn- and Hg-substituted proteins; this Fe(II) species accounted for roughly 10% of the total $^{57}$Fe present, and the data gave no indication whether the corresponding A site was empty or occupied by a diamagnetic ion. The majority of the $^{57}$Fe in these samples occupied the A site or both the A and B sites. We note also that all Mössbauer and EPR samples that had been activated and purified by standard procedures[15] contained at most a few percent of unpaired iron of the "$g \sim 4.3$" type and no measurable Fe(II), although the number of irons per enzyme varied between 1.3 and 2 among different preparations. This observation means that there is an efficient exchange of metal ions that allows the protein to form the more stable binuclear clusters at the expense of less stable complexes with a single metal; the preparation-dependent fraction with no iron at all is presumably denatured, or the combination of apoprotein and protein with the binuclear cluster must be more stable than the single-metal complexes.

**Acknowledgment.** This work was supported in part by Grant GM 16406 and in part by grants from the Australian Research Grants Committee and the University of Queensland.

**Registry No.** PAP, 9001-77-8; Fe, 7439-89-6.

(67) Larger differential enrichment (67–33%) was recently reported for PAP from beef spleen (Cichutek, K.; Witzel, H.; Parak, F. *Hyperfine Interact.* **1988**, *42*, 885–888), but comparison with our results is difficult since neither the conditions nor the uncertainties are clearly specified.

# Magnesium Ion Catalyzed P–N Bond Hydrolysis in Imidazolide-Activated Nucleotides. Relevance to Template-Directed Synthesis of Polynucleotides

**Anastassia Kanavarioti,* Claude F. Bernasconi,* Donald L. Doodokyan,[1] and Diann J. Alberas**

*Contribution from the Chemistry Department, University of California, Santa Cruz, California 95064.* *Received February 27, 1989*

**Abstract:** Magnesium, an ion necessary in enzymatic as well as in nonenzymatic template-directed polynucleotide-synthesizing reactions, has been found to catalyze the hydroxide ion attack on the P–N bond of selected 5′-monophosphate imidazolide derivatives of nucleotides, such as guanosine 5′-monophosphate 2-methylimidazolide (2-MeImpG), guanosine 5′-monophosphate imidazolide (ImpG), and adenosine 5′-monophosphate 2-methylimidazolide (2-MeImpA). Calcium ion behaves similarly, but quantitatively the effects are smaller. Pseudo-first-order rate constants of 2-MeImpG and ImpG hydrolysis as a function of $Mg^{2+}$ concentration have been obtained in the range $6 \leq pH \leq 10$ at 37 °C. $Mg^{2+}$ catalysis is particularly effective around pH 10 where a 0.02 M concentration leads to 15-fold acceleration and a 0.2 M concentration to a 115-fold acceleration of the rate. At other pH values $Mg^{2+}$ catalysis is less dramatic, mainly because the noncatalyzed reaction is faster. $Mg^{2+}$ catalysis is attributed to the reaction of the zwitterionic form of the substrate ($SH^{\pm}$, imidazolide moiety protonated) with $OH^-$ rather than reaction of the anionic form ($S^-$, imidazolide moiety deprotonated) with water. This conclusion is based on a study of the N-methylated substrates *N*-MeImpG and 1,2-diMeImpG, respectively, which were generated in situ by the equilibrium reaction of ImpG with *N*-methylimidazole and 2-MeImpG with 1,2-dimethylimidazole, respectively. In contrast, in the *absence* of $Mg^{2+}$ the reaction of $S^-$ with water competes with the reaction of $SH^{\pm}$ with $OH^-$. The present study bears on the mechanism of the $Mg^{2+}$-catalyzed template-directed synthesis of oligo- and polynucleotides derived from 2-MeImpG and on the competition between oligonucleotide synthesis and hydrolysis of 2-MeImpG.

Reactions of imidazolide-activated nucleotides or nucleotide analogs are of interest because these activated monomers have been used successfully in modeling the nonenzymatic, template-directed synthesis of oligonucleotides.[2-4] In these syntheses a poly- or oligonucleotide, acting as the template, directs the polymerization of the complementary mononucleotide on the basis of Watson–Crick base-pairing interactions in a similar fashion as DNA/RNA directs the synthesis of a daughter polynucleotide using triphosphate nucleotides as the activated monomers.[5]

(1) D.L.D. was supported by NASA Grant No. NCC2-166 to the late Prof. D. H. White of the University of Santa Clara.
(2) Kanavarioti, A.; White, D. H. *Origins Life* **1987**, *17*, 333.
(3) Inoue, T.; Orgel, L. E. *Science* **1983**, *219*, 859.
(4) Orgel, L. E. *J. Theor. Biol.* **1986**, *123*, 127.

(5) A complete replication cycle consists of the formation of a daughter strand that is complementary to the template, followed by the use of the daughter strand as template to form its complementary strand, the parent molecule.

0002-7863/89/1511-7247$01.50/0 